Coordinated chassis control of a tractor-semitrailer combination operating at its handling limits using the MHA methodology

N.B. When citing this work, cite the original published paper.

(article starts on next page)

Coordinated chassis control of a tractor-semitrailer combination operating at its handling limits using the MHA methodology

Aria Noori Asiabar, Timothy Gordon, Yangyan Gao, Leon Henderson & Leo Laine

Published online: 17 Jun 2024.

Submit your article to this journal ⬀

Article views: 913

View related articles ⬀

View Crossmark data ⬀

Citing articles: 6 View citing articles ⬀

Coordinated chassis control of a tractor-semitrailer combination operating at its handling limits using the MHA methodology

Aria Noori Asiabar[a], Timothy Gordon[a], Yangyan Gao[b], Leon Henderson[c,d] and Leo Laine[c,d]

[a]University of Lincoln, Lincoln, UK; [b]Volvo Group North America LLC, NC, USA; [c]Volvo Group Trucks Technology, Gothenburg, Sweden; [d]Chalmers University of Technology, Gothenburg, Sweden

ABSTRACT

The performance benefits associated with coordinated control of a tractor-semitrailer combination are tested in this paper. More specifically, the paper evaluates performance as the number of available actuators is varied. Coordinating a large number of actuators to control articulated vehicles is a challenging task. To tackle this challenge effectively, a method that can be consistently applied across various levels of actuation is required. The modified Hamiltonian Algorithm (MHA) methodology is found to be suitable for the analysis. The method employs a multivariable nonlinear controller to provide steering and braking actuator inputs for simultaneous stability control and path following for articulated vehicles, even when operating in the nonlinear region of the tyres. This paper specifically investigates the potential performance benefits of using individual wheel braking compared to having limited control with regard to the semitrailer under challenging conditions. To achieve this, the original MHA technique is extended to be applicable to articulated vehicles. As a benchmark scenario, an autonomous safety-critical lane change manoeuvre on a low-friction road is performed by using a relatively simple steering controller. Simulation is conducted through co-simulation of Matlab/Simulink and TruckMaker. Results show that using individual wheel brake actuators for both units combined with automated steering can offer significant performance advantages compared to simpler chassis control strategies.

1. Introduction

The tractor-semitrailer combination plays an important role in road transportation due to its high efficiency and cost-effectiveness. Compared to single-unit heavy goods vehicles, the tractor-semitrailer combination is articulated and more susceptible to undesirable behaviour when travelling at high speeds or on low-friction surfaces especially when it is fully loaded [1]. In a well-known study of crash data [2], the datasets showed that the loss of stability is a major factor in many tractor-semitrailer accidents. When it comes

CONTACT Aria Noori Asiabar ✉ anoori@lincoln.ac.uk

to handling performance, a tractor towing a trailer may encounter adverse conditions due to poorly controlled trailer dynamics. A tractor-semitrailer combination is also a more complex system than single-unit vehicles, necessitating a more advanced control architecture [1].

It is now well established from a variety of studies that using driver assistant systems can reduce the risk of articulated vehicles crashes [2]. The motion control of the tractor-semitrailer combinations has been the subject of many studies [3–8]. However, the potential benefits of expanding the number of semitrailer actuators accessible to a centralised motion controller are not addressed adequately.

Currently, the primary focus of active controls for articulated vehicles is directed towards the tractor unit, especially through individual wheel braking via direct yaw motion control. Some existing literature also explores the concept of using differential braking to control the semitrailer unit [4,9–26]. The research in [23] presented a technique for improving the stability of a two-axle tractor and a three-axle semitrailer combination during high-speed evasive manoeuvres. The control strategy included monitoring the yaw rate difference between the tractor and semitrailer and activating differential braking on the semitrailer when the articulation rate exceeded a certain threshold.

Lateral stability control of a tractor-semitrailer combination is investigated in [27], especially with a focus on parametric uncertainties. The control technique used is the Robust Linear Quadratic Regulator (RLQR) considering the uncertainties in the vehicle parameters such as payload. For performance comparison, the H_∞ robust control technique is used. The effectiveness of both controllers was tested in a double lane-change scenario. Simulation results indicate that RLQR approach outperformed H_∞ in terms of lateral stability.

Controlling an additional yaw moment is normally key to the effective implementation of the differential braking control. Furthermore, there are parameter uncertainties as well as unmodelled dynamics which require the control algorithms to be robust or adaptive. In [20] the authors presented a novel control scheme for improving the yaw stability of a tractor-semitrailer combination in critical situations. The presented control structure has two layers: an upper yaw moment controller and a lower brake force distributor. The tractor and semitrailer are independently stabilised using fuzzy logic-based yaw moment controllers. These controllers are intended to track the tractor's reference yaw rate and the articulation angle between the tractor and the semitrailer while accounting for variations in the articulation angular rate. The control scheme is shown to be robust and effective in stabilising severe instabilities such as jackknife and trailer oscillation, according to simulations using a nonlinear vehicle model. The dynamics and stability of a tractor-semitrailer combination are also the focus of [21]. Based on nonlinear dynamics analysis, the study examines and discusses jackknife, trailer swing, and trailer oscillation using Sliding Mode Control (SMC). Simulations, using a comprehensive nonlinear vehicle model, showed good control performance, and a certain level of robustness when the trailer load changed. In [16], the performance of two controllers was compared for a tractor-trailer combination. These were: a state feedback controller with an integral action and SMC. Simulations were used to evaluate various driving scenarios such as braking and accelerating on a dry road and a double-lane change manoeuvre on a slippery road. According to the results, SMC outperformed the state feedback controller by closely following a desired path in these driving manoeuvres.

Model Predictive Control (MPC) is another method used to address these problems, especially in order to calculate the additional yaw moment. In [26], researchers developed a suitable MPC for controlling a car-trailer combination. The controller design utilised a three-degrees-of-freedom planar bicycle model, and the results indicate that the MPC controller's design effectively mitigates instability modes. In [28], a universal and reconfigurable motion control structure for articulated vehicles was presented. In the upper layer, MPC is designed to evaluate a set of desired global forces and moments for each unit. Then, a quadratic programming optimisation-based control allocation is used to provide the steering and braking requests for the wheels. For enhancing maneuverability and path-tracking of a tractor-semitrailer combination a model predictive control method with an optimal curvature preview technique is employed [29]. The co-simulation of MATLAB/SIMULINK and TruckSim validates the performance improvement. While the proposed controller demonstrates satisfactory performance under low lateral acceleration, it may struggle when dealing with highly nonlinear lane changes. In terms of integrated control, the stability of a tractor-semitrailer combination is improved through the use of the Nonlinear Model Predictive Control (NMPC) technique in [30]. Simulations validate the performance of the proposed NMPC controller for a predefined path. However, the adjustment of NMPC parameters appears to be manoeuvre-specific, suggesting that for each new manoeuvre, the crucial parameters influencing performance may need modification. Such fine-tuning will pose serious challenges for real-time applications, as does the computational complexity of NMPC.

Clearly, for safety-critical manoeuvres, a simple linear model is not sufficient to represent force control at the limits of adhesion. Although many authors approximate the nonlinear tyre characteristics using local linearization [9–11,13,18,27,31,32], others will make use of a full nonlinear model [30,33,34] as this eliminates any concern over the effects of linearization. In particular, MHA makes full use of a nonlinear tyre model without any excessive computational cost [34,35]. Also, the role of articulation forces is not fully considered in many of these studies.

Looking to the future, the ability to independently control the brakes on each wheel of a tractor-semitrailer combination will require sophisticated nonlinear multivariable control systems. Based on the literature reviewed, it is reasonable to expect that such control systems will bring additional benefits for safety. On the other hand, as the number of articulated units and actuators increases, there must be a concern that vehicle control algorithms become increasingly complex and potentially unreliable. An example would be where numerical optimisation within the control loop fails to converge within the available time.

The key question addressed in this paper is the degree to which coordinating an increasing number of actuators will improve stability and directional control for articulated vehicles, with a focus on the tractor-semitrailer combination. In following this approach a number of original contributions are made and these are summarised in the Conclusions and further discussion section.

A consistent control approach is required as increasing levels of control authority are considered. The Modified Hamiltonian Algorithm (MHA) is used for this purpose because of its computational simplicity (relative to MPC and other optimising methods) and the seamless way it deals with variable actuator combinations.

In previous work [34,36–38], the MHA methodology has been shown to be a suitable approach to designing control systems for light vehicles. Developing the MHA formulation to be fully applicable to the tractor-semitrailer combination is a key development presented in this paper. Note that, in related work [35], the authors tested MHA in real-world experiments, there for both tractor and tractor-semitrailer combinations.

In this research, we explore how the performance of the tractor-semitrailer combination control changes based on the number of available actuators. The baseline scenario involves executing a fast autonomous lane change based on a time-based desired lateral offset on a low-friction surface ($\mu = 0.3$) using the Pure Pursuit (PP) algorithm. Various levels of brake system support for the PP algorithm are considered, from independent wheel braking on all wheels of the tractor up to individual wheel braking for all wheels of tractor semitrailer. The performance of the control system is further evaluated when the MHA is given the authority to front-axle steering as opposed to the PP algorithm.

In the following section, the PP steering controller is presented, and then in Section 3, the focus will be on solving the motion control problem using the MHA methodology. This involves extending previous formulations to include the effect of the articulation joint. Section 4 addresses the core of the paper; comparing in simulation the differences between full coordination, and partial coordination across all actuators. Finally, in Section 5 conclusions and further research challenges will be highlighted.

2. Pure Pursuit steering controller

The PP algorithm is widely used in the literature, offering robust performance, simplicity and a minimal parameter tuning set [39]. It involves defining a Goal Point (GP) located some distance ahead of the vehicle on a desired path. The front axle steering angle is selected in such a way as to direct a reference point on the vehicle towards the GP on the path based on a kinematic bicycle model. While PP is based on kinematic principles, it has previously been used for dynamic closed-loop manoeuvres [40–42]. The motivation is to use a simple reference that can be indicative of reasonable driver behaviour or a simple automated driving system.

The PP algorithm used in this paper considers the centre of the rearmost axle of the tractor as the reference point (shown in Figure 1) targeted towards a constant radius arc that ends at the GP.

From Figure 1 we have:

$$\tan \gamma = \frac{Y_{GP} - Y_R}{X_{GP} - X_R} = \frac{Y_{GP} - Y_R}{L_p} \tag{1}$$

Here, $\gamma = \alpha + \psi$ and the preview distance (L_p) is a parameter that can be adjusted based on the vehicle's speed. Following common practice [43] we define $L_p = \tau_p U$ where τ_p is a preview time and U is the vehicle longitudinal speed. The straight-line distance to the GP (l_d) is then calculated as:

$$l_d = \sqrt{(Y_{GP} - Y_R)^2 + L_p^2} \tag{2}$$
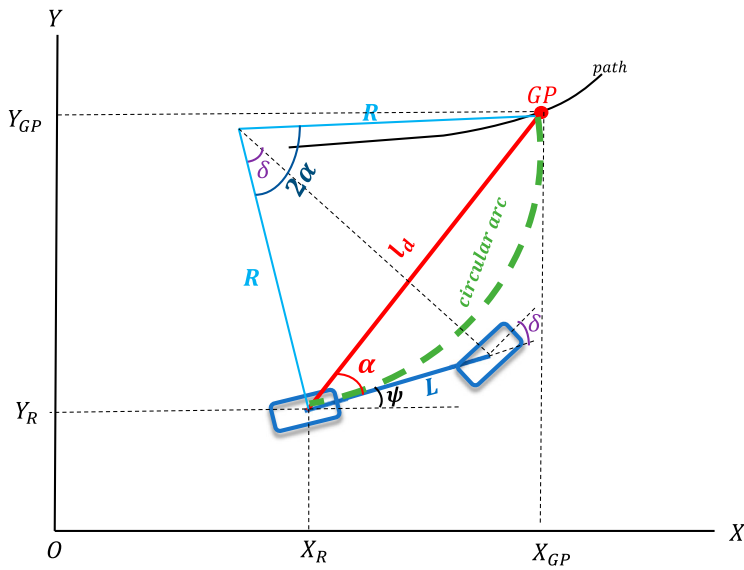
Figure 1. Schematic of PP algorithm derivation (*L* is the vehicle wheelbase).

Because the triangle in Figure 1 is isosceles, according to the law of sines we can write for the desired radius of curvature:

$$R_{des} = \frac{l_d}{2 \sin \alpha} \tag{3}$$

From the kinematic bicycle model [44], the front axle steer angle is expressed as $\delta = \arctan(L/R)$. Combining this with Equation (3) the front axle steer angle needed to reach the GP is then written as:

$$\delta_{des} = \tan^{-1} \frac{L}{R_{des}} = \tan^{-1}(L\kappa_{des}) \tag{4}$$

where $\kappa_{des} = 1/R_{des}$ is the desired curvature of the arc.

The reference lateral offset for an evasive lane change is conveniently defined by a 5th-order polynomial [45]:

$$Y_d(t) = a_1 t^5 + a_2 t^4 + a_3 t^3 + a_4 t^2 + a_5 t + a_6 \tag{5}$$

The coefficients in Equation (5) are obtained by applying initial and final conditions at times t_0 and t_f respectively assuming a desired lateral offset of 3.5 metres:

$$\begin{aligned} Y_d(t_0) = 0, \quad \dot{Y}_d(t_0) = 0, \quad \ddot{Y}_d(t_0) = 0 \\ Y_d(t_f) = 3.5 \quad \dot{Y}_d(t_f) = 0 \quad \ddot{Y}_d(t_f) = 0 \end{aligned} \tag{6}$$

Figure 2. The desired lateral offset signifying an evasive lane change manoeuvre for the centre of the rearmost axle of the tractor followed by PP.

These conditions imply:

$$
\begin{bmatrix}
t_0{}^5 & t_0{}^4 & t_0{}^3 & t_0{}^2 & t_0 & 1 \\
t_f{}^5 & t_f{}^4 & t_f{}^3 & t_f{}^2 & t_f & 1 \\
5t_0{}^4 & 4t_0{}^3 & 3t_0{}^2 & 2t_0{}^2 & 2 & 0 \\
5t_f{}^4 & 4t_f{}^3 & 3t_f{}^2 & 2t_f{}^2 & 2 & 0 \\
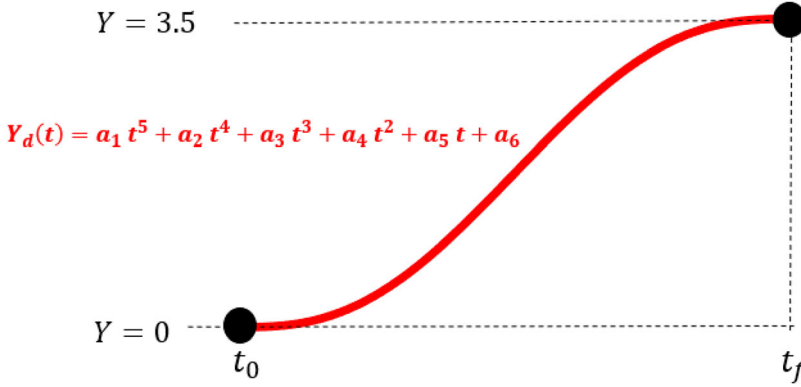20t_0{}^3 & 12t_0{}^2 & 6t_0{}^2 & 20 & 0 & 0 \\
20t_f{}^3 & 12t_f{}^2 & 6t_f{}^2 & 20 & 0 & 0
\end{bmatrix}
\begin{bmatrix}
a_1 \\ a_2 \\ a_3 \\ a_4 \\ a_5 \\ a_6
\end{bmatrix}
=
\begin{bmatrix}
0 \\ 3.5 \\ 0 \\ 0 \\ 0 \\ 0
\end{bmatrix}
\tag{7}
$$

The coefficients are subsequently calculated offline to establish a reference for the vehicle to follow. A schematic of the time-based desired lateral offset can be seen in Figure 2.

3. Coordinated chassis control using MHA

MHA is based on Pontryagin's Minimum Principle (PMP) method within the realm of nonlinear optimal control theory [46]. According to PMP, as long as the co-states of the system dynamics are calculated correctly, the minimisation of the overall cost function is obtained simply by minimizing the current scalar Hamiltonian function subject to any actuator constraints at each time step. However, calculating the co-states of the Hamiltonian function using PMP results in solving a Two-point Boundary Value Problem (2PBVP) as described in [46] which makes the computation difficult in real-time. Therefore, in the formulation of MHA, the co-states are estimated based on simple dynamic principles, which greatly simplifies the problem but may result in a suboptimal solution. The co-state estimation considers the desired trajectory as well as yaw and sideslip stability.

A global Hamiltonian is constructed using global forces and moments, which are considered as generalised forces or virtual controls. The formulation assumes there are no cost penalties associated with the virtual controls; instead, constraints are applied at the wheel level. As a result, when incorporating the estimated co-states, the Hamiltonian H becomes linear in terms of the generalised forces. In turn, H is decomposed into individual wheel force contributions, greatly simplifying the global coordinated control problem.

Alternative methods for finding the co-states have been applied to vehicle motion control. Yang et al. [47] used a brake-based path controller through the quasi-linear optimal

control (QLOC) method for reducing the possibility of secondary collisions after an initial impact. However, QLOC requires the solution of the full nonlinear state-space equations to be performed at each time step, increasing the complexity and computing requirements.

MHA for single-unit vehicles was first formulated in [36,37], and further applied in [34,38]. The control architecture of MHA consists of two levels, and in the present work, this is fully retained. The upper level generates a reference for longitudinal and lateral accelerations, while the lower level divides the optimal motion control into separate sub-problems to be solved locally for each wheel. For the articulated vehicle, the acceleration reference is applied only to the tractor, while yaw motion control is applied to both units.

3.1. High-level reference generation

As mentioned, MHA requires a desired acceleration vector as input. When PP controls front axle steering, this may be found from the desired curvature (κ_{des}) obtained from PP:

$$a_{Y_d} = \kappa_{des}U^2 \tag{8}$$

For the present study, which assumes a low-friction road surface, a saturation limit of 0.3 g is imposed on a_{Y_d}, which is resolved normal to the direction of the road, and a_{X_d} is assumed zero.

When PP is replaced by the MHA steering control, an SMC method is used [48]. The motivation for employing SMC is the need for a more aggressive lane change when executing an obstacle avoidance manoeuvre within a specific time frame. SMC here is used to set the reference acceleration of the centre of gravity (CG) of the tractor, as required to track the desired lateral offset defined in Equation (5). The sliding surface is defined as:

$$S = \left(\frac{d}{dt} + \eta\right)\tilde{y} \tag{9}$$

where $\tilde{y} = Y_{G_1} - Y_d$ is the lateral position error and Y_{G_1} is the tractor's CG lateral displacement, Y_d is the tractor's CG desired lateral offset and η is a positive constant. Taking the derivative of Equation (9), we have

$$\dot{S} = \ddot{Y}_{G_1} - \ddot{Y}_d + \eta\left(\dot{Y}_{G_1} - \dot{Y}_d\right) \tag{10}$$

Then u_{equ} is the equivalent control input that makes the $\dot{S}$ become zero:

$$u_{equ} = \ddot{Y}_d - \eta\left(\dot{Y}_{G_1} - \dot{Y}_d\right) \tag{11}$$

Based on SMC theory [48]:

$$u = u_{equ} - K_{SMC}sgn(S) \tag{12}$$

Here $u = a_{Y_d}$ is the desired lateral acceleration for MHA replacing Equation (8), and K_{SMC} is a gain for the discontinuous *sign* function. After some coordinate transformations, this can be written as:

$$a_{Y_d} = \ddot{Y}_d - \eta\left(v_{y_1}\cos\psi_1 + v_{x_1}\sin\psi_1 - \dot{Y}_d\right) - K_{SMC}sgn(S) \tag{13}$$

where v_{x_1} and v_{y_1} are respectively the components of the velocity vector of the tractor CG in vehicle coordinates and ψ_1 is the tractor yaw angle. As is common in SMC, a saturation

function is used in place of the discontinuous sign function, to avoid excessive chattering [48]:

$$a_{Y_d} = \ddot{Y}_d - \eta \left(v_{y_1} \cos \psi_1 + v_{x_1} \sin \psi_1 - \dot{Y}_d \right) - K_{SMC} sat \left(\frac{S}{\phi} \right) \tag{14}$$

and ϕ is the thickness of the boundary layer.

3.2. Hamiltonian formulation

The equations of motion (EOM) for the tractor-semitrailer combination using Euler-Lagrange [49] formulation are written as:

$$\frac{d}{dt} \left(\frac{\partial L}{\partial \dot{q}_k} \right) - \frac{\partial L}{\partial q_k} = Q_{q_k} \tag{15}$$

Here the Lagrangian is $L = T - V$, where T is the kinetic energy and V is the system's potential energy, which is zero in this case. Also, Q_{q_k} is the generalised force which is the force conjugate to the coordinate q_k. Here the generalised coordinates are defined as:

$$\vec{q} = \begin{pmatrix} X_{G_1} & Y_{G_1} & \psi_1 & \psi_2 \end{pmatrix}^T \tag{16}$$

where X_{G_1} and Y_{G_1} denote the tractor CG coordinates, and ψ_1 and ψ_2 represent the yaw angles of the tractor and semitrailer respectively. By applying Equation (15) to each generalised coordinate, the EOM can be written as:

$$M(q)\ddot{\vec{q}} + C(\vec{q}, \dot{\vec{q}}) = \vec{Q} \tag{17}$$

Written in detail:

$$\begin{bmatrix} m_1 + m_2 & 0 & m_2 b_1 \sin \psi_1 & m_2 a_2 \sin \psi_2 \\ 0 & m_1 + m_2 & -m_2 b_1 \cos \psi_1 & -m_2 a_2 \cos \psi_2 \\ m_2 b_1 \sin \psi_1 & -m_2 b_1 \cos \psi_1 & I_{zz_1} + m_2 b_1^2 & b_1 m_2 a_2 \cos(\psi_1 - \psi_2) \\ m_2 a_2 \sin \psi_2 & -m_2 a_2 \cos \psi_2 & b_1 m_2 a_2 \cos(\psi_1 - \psi_2) & I_{zz_2} + m_2 a_2^2 \end{bmatrix} \begin{bmatrix} \ddot{X}_1 \\ \ddot{Y}_1 \\ \ddot{\psi}_1 \\ \ddot{\psi}_2 \end{bmatrix}$$

$$+ \begin{bmatrix} b_1 m_2 \cos \psi_1 \dot{\psi}_1^2 + a_2 m_2 \cos \psi_2 \dot{\psi}_2^2 \\ b_1 m_2 \sin \psi_1 \dot{\psi}_1^2 + a_2 m_2 \sin \psi_2 \dot{\psi}_2^2 \\ a_2 b_1 m_2 \sin(\psi_1 - \psi_2) \dot{\psi}_2^2 \\ -a_2 b_1 m_2 \sin(\psi_1 - \psi_2) \dot{\psi}_1^2 \end{bmatrix} = \begin{bmatrix} Q_{X_1} \\ Q_{Y_1} \\ Q_{\psi_1} \\ Q_{\psi_2} \end{bmatrix}$$

Rewriting Equation (17):

$$\ddot{\vec{q}} = -M^{-1} C(\vec{q}, \dot{\vec{q}}) + M^{-1} \vec{Q} \tag{18}$$

For the optimal control formulation, we require a state vector $\vec{x}$ consisting of coordinates and velocities, typically $\vec{x} = \begin{bmatrix} \vec{q} & \dot{\vec{q}} \end{bmatrix}^T$. However, using the available freedom in the choice

of state variables, we define the state vector as:

$$\vec{x} = \begin{bmatrix} \vec{x}_a \\ \vec{x}_b \end{bmatrix} = \begin{bmatrix} \vec{q} \\ K\dot{\vec{q}} \end{bmatrix}, \quad K = \begin{bmatrix} m_1 & 0 & 0 & 0 \\ 0 & m_2 & 0 & 0 \\ 0 & 0 & \dfrac{I_{z_1}}{k_1} & 0 \\ 0 & 0 & 0 & \dfrac{I_{z_2}}{k_2} \end{bmatrix} \tag{19}$$

where k_1 and k_2 are the radii of gyration for the tractor and the semitrailer units respectively. Written in detail:

$$\vec{x} = \begin{bmatrix} \vec{x}_a \\ \vec{x}_b \end{bmatrix} = \begin{bmatrix} X_{G_1} & Y_{G_1} & \psi_1 & \psi_2 & m_1\dot{X}_{G_1} & m_1\dot{Y}_{G_1} & \dfrac{I_{z_1}}{k_1}\dot{\psi}_1 & \dfrac{I_{z_2}}{k_2}\dot{\psi}_2 \end{bmatrix}^T \tag{20}$$

According to this definition, all the components of vector $\dot{\vec{x}}_b$ have the dimension of force rather than a combination of forces and moments. This distinction will be advantageous when decomposing the Hamiltonian function later. This choice also aligns more closely with the earlier version of MHA presented in [37]. From Equations (18) and (19) the state equations are:

$$\dot{\vec{x}}_a = K^{-1}\vec{x}_b \tag{21}$$

$$\dot{\vec{x}}_b = K\ddot{\vec{q}} = -KM^{-1}\vec{C} + KM^{-1}\vec{Q} \tag{22}$$

The forcing term involving Q in Equation (22) is considered as a set of generalised forces:

$$\vec{V} = KM^{-1}\vec{Q} = \begin{bmatrix} v_1 & v_2 & v_3 & v_4 \end{bmatrix}^T \tag{23}$$

Then the scalar Hamiltonian function from optimal control theory [46] is written as:

$$H = \vec{\lambda}^T\dot{\vec{x}} = \vec{\lambda}^T f(\vec{x}, \vec{u}) \tag{24}$$

where $\vec{\lambda}$ is the co-state vector. Now, from Equation (19) the Hamiltonian takes the form:

$$H = \vec{\lambda}^T\dot{\vec{x}} = \vec{\lambda}_a^T\dot{\vec{x}}_a + \vec{\lambda}_b^T\dot{\vec{x}}_b \tag{25}$$

where

$$\vec{\lambda}_a = \begin{bmatrix} \lambda_1 & \lambda_2 & \lambda_3 & \lambda_4 \end{bmatrix}^T, \quad \vec{\lambda}_b = \begin{bmatrix} \lambda_5 & \lambda_6 & \lambda_7 & \lambda_8 \end{bmatrix}^T$$

It is important to remind that while the elements within $\vec{V}$ are described as generalised forces, they all possess the units of force. Substituting Equation (22) and (21) in Equation (25) we obtain:

$$H = \vec{\lambda}_a^T K^{-1}\vec{x}_b + \vec{\lambda}_b^T(-KM^{-1}\vec{C} + \vec{V}) \tag{26}$$

Since the purpose is to minimise H to obtain actuator commands, only the final term is of interest:

$$H_{active} = \vec{\lambda}_b^T\vec{V} = \lambda_5 v_1 + \lambda_6 v_2 + \lambda_7 v_3 + \lambda_8 v_4 \tag{27}$$

Then, H_{active} is to be minimised subject to constraints to determine the actuator commands.

3.3. Modified Hamiltonian

As mentioned, in MHA, rather than solving a 2PBVP to determine the co-states in Equation (27), physical principles and heuristics are used to perform an estimation. As in the case of single-unit vehicles [34,37], the first two terms in the Hamiltonian Equation (27) are determined by considering the dynamics of the CG of the tractor in the absence of significant yaw dynamics. Thus, minimizing H_{active} is equivalent to maximising the force component, and hence the acceleration, in the opposite direction of $\begin{bmatrix} \lambda_5 & \lambda_6 \end{bmatrix}^T$. In other words, we choose $\begin{bmatrix} \lambda_5 & \lambda_6 \end{bmatrix}^T = -\vec{a}_d$.

It is important to note that the overall magnitude of H_{active} is unimportant; it can be multiplied by any positive scalar and the optimisation results are unaffected. As a result, we are free to normalise the Hamiltonian in Equation (27) and in MHA we replace the $\begin{bmatrix} \lambda_5 & \lambda_6 \end{bmatrix}^T$ by $\begin{bmatrix} P_X & P_Y \end{bmatrix}^T$ and we set:

$$P_X = -\hat{a}_{X_d}, \quad P_Y = -\hat{a}_{Y_d} \tag{28}$$

in order to maximise the acceleration in the direction of $\vec{a}_d$. This will be subject to the actuator and friction constraints. Here $\hat{a}_d$ is the normalised acceleration target. Therefore, P_X and P_Y are defined as:

$$P_X = -\hat{a}_{X_d} = -\frac{a_{X_d}}{\sqrt{a_{X_d}{}^2 + a_{Y_d}{}^2}}, \quad P_Y = -\hat{a}_{Y_d} = -\frac{a_{Y_d}}{\sqrt{a_{X_d}{}^2 + a_{Y_d}{}^2}} \tag{29}$$

where a_{X_d} and a_{Y_d} are longitudinal and lateral components of the desired acceleration vector in global coordinates.

Therefore, the Hamiltonian in Equation (27) is written as:

$$H_{active} = P_X v_1 + P_Y v_2 + P_{Z_1} v_3 + P_{Z_2} v_4 \tag{30}$$

The co-states P_X, P_Y, P_{Z_1} and P_{Z_2} are considered dimensionless and the generalised forces $v_1, \ldots, v_4$ are all have force dimension $[N]$. Therefore, the dimension of the Hamiltonian in Equation (30) is $[N]$.

The P_Z variables, yet to be defined play the crucial role as trade-off functions, determining the instantaneous balance between maximising the acceleration of the mass centre and controlling the yaw dynamics of the relevant unit.

A target yaw rate in MHA is computed in real-time, considering the anticipated path curvature and the desired body sideslip, as outlined in Appendix 3. Comparing this to the actual yaw rate, a corresponding desired yaw moment, $M_{z_i}{}^d$, is found, and trade-off parameters P_Z are adjusted to guide the actual yaw motion towards the reference as:

$$M_{z_i}^{err} = \frac{M_{z_i} - M_{z_i}{}^d}{|M_{z_i}| + |M_{z_i}{}^d| + \epsilon} \tag{31}$$

$$P_{Z_i}(k+1) = \text{sat}\left\{ P_{Z_i}(k) + K_i \tanh M_{z_i}^{err}(k) \right\} \tag{32}$$

where

$$\text{sat}(x) = \begin{cases} -1 & x \le -1 \\ x & -1 < x < 1 \\ 1 & x \ge 1 \end{cases} \tag{33}$$

Here i is the index for the number of units, and ϵ is a small parameter used to avoid possible division by zero. The adaptation gains K_i is one of the most important tuning parameters in the MHA algorithm which directly affects the MHA performance. Also the M_z^{err} is the difference between the yaw moment prediction from MHA and the desired yaw moment and it is constrained in the range of ± 1. According to Equation (32), P_{Z_i} is likewise constrained in the range ± 1. Then, in order for yaw control to be capable of dominating the terms in H_{active}, the following transformation is included:

$$\Lambda_i = \frac{P_{Z_i}}{1 - |P_{Z_i}| + \epsilon} \tag{34}$$

where ϵ is a small constant. As a result, the Hamiltonian in Equation (30) is written as :

$$H_{active} = P_X v_1 + P_Y v_2 + \Lambda_1 v_3 + \Lambda_2 v_4 \tag{35}$$

The desired acceleration vector in the previous section is then targeted, together with yaw motion control targets, through the minimisation of the Hamiltonian function denoted as Equation (35) employing both steering and braking actuators. To determine actuator commands, we now cascade Equation (35) into component wheel-level Hamiltonians.

3.4. Control allocation through scalar Hamiltonian decomposition

Due to Hamiltonian's linearity with respect to the virtual controls in Equation (35), and also the linearity of virtual controls with respect to tyre forces, we now resolve H_{active} into discrete contributions from each wheel. Writing the Hamiltonian in Equation (35) as:

$$H_{active} = \vec{P}^{gT} \vec{V} = \vec{P}^{gT} K M^{-1} \vec{Q} \tag{36}$$

Here $\vec{P}^g = (P_X \ P_Y \ \Lambda_1 \ \Lambda_2)^T$ and the superscript g denotes the use of global (inertial) coordinates. Now the generalised forces $\vec{Q}$ can be written in terms of the individual tyre forces F_{ij} as:

$$\vec{Q} = \sum_{i=1}^{2} \sum_{j=1}^{6} [B]_{ij} \vec{F}_{ij} \tag{37}$$

The indices i and j are associated with units and wheels in each unit, respectively, and $[B]_{ij}$ is the input Jacobian matrix written in full in the Appendix 2. The Hamiltonian in

Equation (36) considering Equation (37) is then written as:

$$H_{active} = \vec{P}^{gT} K M^{-1} \sum_{i=1}^{2} \sum_{j=1}^{6} [B]_{ij} \vec{F}_{ij} \tag{38}$$

The decomposition is then obtained as:

$$H_{active} = \sum_{i=1}^{2} \sum_{j=1}^{6} \vec{\tilde{P}}^{g}_{ij}{}^{T} \vec{F}_{ij} \tag{39}$$

where

$$\vec{\tilde{P}}^{g}_{ij}{}^{T} = \vec{P}^{g} K M^{-1} [B]_{ij} \tag{40}$$

This achieves the decomposition and minimisation of H_{active} is now reduced to the parallel minimisation of each H_{ij}. Using the dot product we can write:

$$H_{ij} = \begin{bmatrix} \tilde{P}^{g}_{x_{ij}} \\ \tilde{P}^{g}_{y_{ij}} \end{bmatrix} \cdot \begin{bmatrix} F_{x_{ij}}{}^{g} \\ F_{y_{ij}}{}^{g} \end{bmatrix} = \vec{\tilde{P}}^{g}_{ij} \cdot \vec{F}^{g}_{ij} \tag{41}$$

Here the H_{ij} has the dimension of force the same as $\vec{F}^{g}_{ij}$ while $\vec{\tilde{P}}^{g}_{ij}$ is dimensionless. The dot product in H_{ij} is preferentially rotated into tyre coordinates:

$$H_{ij} = \vec{\tilde{P}}^{t}_{ij} \cdot \vec{F}^{t}_{ij} \rightarrow \min \tag{42}$$

where $\vec{\tilde{P}}^{t}_{ij}$ is obtained as:

$$\vec{\tilde{P}}^{t}_{ij} = \begin{bmatrix} \cos(\psi_i + \delta_{ij}) & \sin(\psi_i + \delta_{ij}) \\ -\sin(\psi_i + \delta_{ij}) & \cos(\psi_i + \delta_{ij}) \end{bmatrix} \vec{\tilde{P}}^{g}_{ij} \tag{43}$$

At each wheel, the local Hamiltonian in Equation (42) takes the general form $h = p_x F_x + p_y F_y$, written in tyre coordinates and simply the minimisation is done based on the tyre model. This completes the decomposition step. A summary of the MHA controller structure is shown in Figure 3.

The goal is to minimise each specific part of the Hamiltonian function while considering limitations related to surface friction, actuator capability and any imposed tyre force limits. The algorithm's computational simplicity allows for distributing optimisation tasks to individual wheels, which in turn enables the utilisation of a comparatively sophisticated tyre model during the minimisation process.

3.5. Actuator commands

Minimization of the tyre-level local Hamiltonian is based on selecting and controlling both slip angle and slip ratio. As in [37], the wheel rotational dynamics are considered to be much

Figure 3. Modified Hamiltonian Algorithm structure.

faster than the control of slip angle via steering or body yaw motion. Hence

$$S_{x_{ij}}^\star = \arg\min_{S_{x_{ij}}} H_{ij} \qquad (44)$$

As a result, the predicted longitudinal and lateral forces for the optimised slip ratio and given current slip angle are obtained using a combined-slip Magic Formula tyre model:

$$F_{x_{ij}}^p = F_{x_{ij}}(S_{x_{ij}}^\star, \alpha_{ij}), \quad F_{y_{ij}}^p = F_{y_{ij}}(S_{x_{ij}}^\star, \alpha_{ij}) \qquad (45)$$

Under the assumption of an equilibrium state in the wheel dynamics, the corresponding optimised braking torque $T_{b_{ij}}^\star$ is calculated as $T_{b_{ij}}^\star = R_w F_{x_{ij}}^p$, where $R_{w_{ij}}$ is the effective wheel radius for each wheel.

It is important to highlight that the design of the MHA controller considers the presence of multiple time-scale dynamics. In particular, wheel rotational dynamics are considered to be faster than vehicle yaw dynamics, and hence wheel longitudinal slip control runs on a faster time-scale than lateral slip control. Consequently, the $F_{x_{ij}}^p$ can be rapidly obtained.

Once the optimal slip ratio is found, then slip angles are adjusted based on a gradient method. Accordingly, a numerical estimate is obtained using an internal combined-slip tyre model [37,38]. The slip angle α_{ij} is calculated as:

$$\alpha_{ij} \simeq \delta_{ij} + \beta_i - \frac{L_{x_{ij}} \dot{\psi}_i}{v_{x_i}} \qquad (46)$$

In Equation (46), $L_{x_{ij}}$ represents the longitudinal distance from the CG of each unit to each individual wheel. It is evident that the slip angle can be increased or decreased by (i) actively controlling the wheel angle, or (ii) changing the body sideslip angle (β) of the vehicle.

For the tractor-semitrailer combination, equipped with front-wheel steering, the effect of changing the wheel angle and body sideslip angle on the Hamiltonian minimisation can

be expressed via using the chain rule as:

$$H_\delta = \sum_{i=1}^{2}\sum_{j=1}^{6} \frac{\partial H_{ij}}{\partial \delta_{ij}} = \frac{\partial H_{11}}{\partial \alpha_{11}}\frac{\partial \alpha_{11}}{\partial \delta_{11}} + \frac{\partial H_{12}}{\partial \alpha_{12}}\frac{\partial \alpha_{12}}{\partial \delta_{12}} \approx \frac{\partial H_{11}}{\partial \alpha_{11}} + \frac{\partial H_{12}}{\partial \alpha_{12}} \tag{47}$$

For obtaining the desired front wheel angle, the local Hamiltonian is minimised through the control law [37,38]:

$$\dot{\delta}_{des} = -K_{\delta_1}\tanh(K_{\delta_2}H_\delta) \tag{48}$$

Here K_{δ_1} is a maximum steering rate and K_{δ_2} is a gain factor. The parameters K_{δ_1} and K_{δ_2} together affect the aggressiveness of MHA steering action. In a similar way to obtaining H_δ, H_β is found and the desired sideslip angle rate is obtained (Appendix 3).

It is important to highlight that MHA controls the sideslip angle within bounds to optimise the utilisation of tyre forces at the unsteered axles, as opposed to attempting to simply minimise body sideslip.

4. Safety-critical autonomous lane change scenario

A safety-critical lane change is simulated using IPG Truckmaker. The braking and steering dynamics are represented through transfer functions from the requested to the actual steer angle and brake torque respectively:

$$\frac{\delta_{act}}{\delta_{req}} = \frac{1}{1+\tau_s s}, \quad \frac{T_{b_{act}}}{T_{b_{req}}} = \frac{1}{1+\tau_b s} \tag{49}$$

where vehicle parameters and the parameters τ_s and τ_b are given in Appendix 1.

4.1. Scenario definition

An autonomous safety-critical lane change manoeuvre on the low-friction surface is conducted in a three-second time window in four phases. The surface friction coefficient is 0.3 and is assumed to be known to the MHA controller. The PID controller maintains the speed at 75 km/h before doing the lane change. The speed controller is turned off at the start of the lane change and remains deactivated throughout the rest of the simulation. It is important to highlight that based on some yaw rate and sideslip angle requirements both for the tractor and the semitrailer units, it is calculated that an additional three seconds of stabilising phase are needed before handing back the control authority to the baseline controller.

- Phase 1 (0–10 seconds): driving in a straight line utilizing the PP steering control and the PID speed controller.
- Phase 2 (10–13 seconds): an evasive lane change is executed within a three-second window.

- Phase 3 (13–16 seconds): stabilising phase to ensure the vehicle's stability using MHA braking when available.
- Phase 4 (16–30 seconds): Control authority is handed back exclusively to the PP.

Different levels of control authority are given to MHA as detailed below.

4.2. Control authority cases

Five different cases are simulated in this paper as summarised in Table 1 and Figure 4.

In case A, PP performs the lane change, with no assistance from MHA. In case B, MHA supports PP steering by applying individual wheel braking to the tractor and proportional braking to the semitrailer to avoid an unbraked semitrailer causing additional destabilisation. In case C, PP is supported by MHA commanding individual wheel braking for the tractor and semitrailer. In cases D and E, MHA acts as a fully integrated autonomous motion controller, responsible for both front axle steering and individual wheel braking for the tractor and semitrailer units. In case D the lateral acceleration reference is determined by the PP algorithm, whereas for case E this comes from SMC via Equation (14).

Table 1. Lateral control authority for the tractor-semitrailer combination. PB: semitrailer proportional braking SC: Speed Controller T: Tractor S: Semitrailer.

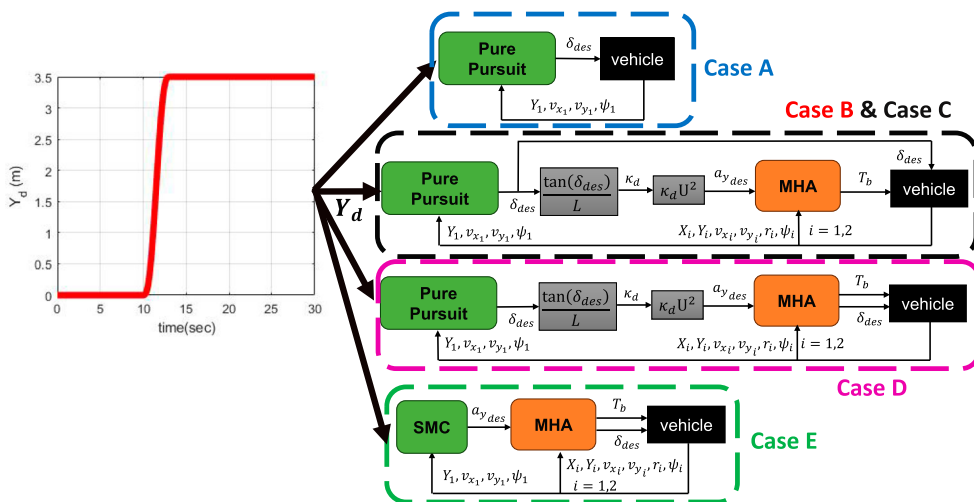| Case	Phase 1	Phase 2,3	Phase 4
A	PP + SC	PP	PP
B	PP + SC	PP + T: MHA S: PB	PP
C	PP + SC	PP + T and S: MHA	PP
D & E	PP + SC	MHA + T and S: MHA	PP

Figure 4. Control authority through different cases.

4.2.1. Proportional braking for the semitrailer

In case B, the proportional braking torque (T_b) for the semitrailer is computed based on the total braking force (F_{b_T}) applied to the tractor by MHA, taking into account the semitrailer vertical static load on each axle (T: Tractor S: Semitrailer i,j: wheel indices).

$$F_{b_{S_j}} = \frac{F_{z_{S_j}}^{static}}{\sum_{i=1}^{6} F_{z_{T_i}}^{static}} F_{b_T} \tag{50}$$

$$T_{b_{S_j}} = F_{b_{S_j}} R_w \tag{51}$$

4.3. Initial simulation results

Simulations were conducted to test the effect of increasing the control authority of MHA. For cases A to D, the time histories are plotted at a specific value of $\tau_p = 1$ second, while in case E, $K_{SMC} = 0.2$ is chosen.

Figure 5 shows lateral deviations (left plots) together with body sideslip angles (right plots). In cases A-D there is a clear trend of improvement with respect to body sideslip, while lateral deviation may show some slight improvement. In case E there is a large improvement in terms of lateral deviation, and an increase in sideslip is seen.

While the PP algorithm focuses on the centre of the rearmost axle for reference tracking during lane changes, lateral offsets of the CG (centre of gravity) are used in the plots. It has been checked that this variation has little effect.

4.4. Trade-off between path-following and lateral stability

The question arises: in case E, is the improvement in path following enough to offset the deterioration in body sideslip control? This cannot be answered with a single 'snapshot' of time histories. Rather, a sequence of simulations is required, showing the trade-off between path following and body sideslip (tracking vs. stability) for each level of actuator authority. For cases with PP steering, improvement in path following can be expected by reducing the preview time τ_p.

The 2D plots in Figure 6 depict the trade-off between minimising tracking error for tractor CG lateral displacement and reducing tractor and semitrailer sideslip angle. Cases A, B, C and D: These cases involve varying the preview time (τ_p) starting from $\tau_p = 3$ seconds and gradually decreasing it until the semitrailer exceeds an assumed maximum sideslip angle of 8 degrees.

- Case A: $\tau_p = 3 : -0.05 : 0.95$ s.
- Case B: $\tau_p = 3 : -0.05 : 0.85$ s.
- Case C: $\tau_p = 3 : -0.05 : 0.8$ s.
- Case D: $\tau_p = 3 : -0.05 : 0.6$ s.

Case E: This case involves varying the gain of the discontinuous function in Sliding Mode Control (K_{SMC}). The range of K_{SMC} values tested is from $0.1 : 0.1 : 0.9$ again with a maximum semitrailer sideslip of 8 degrees.
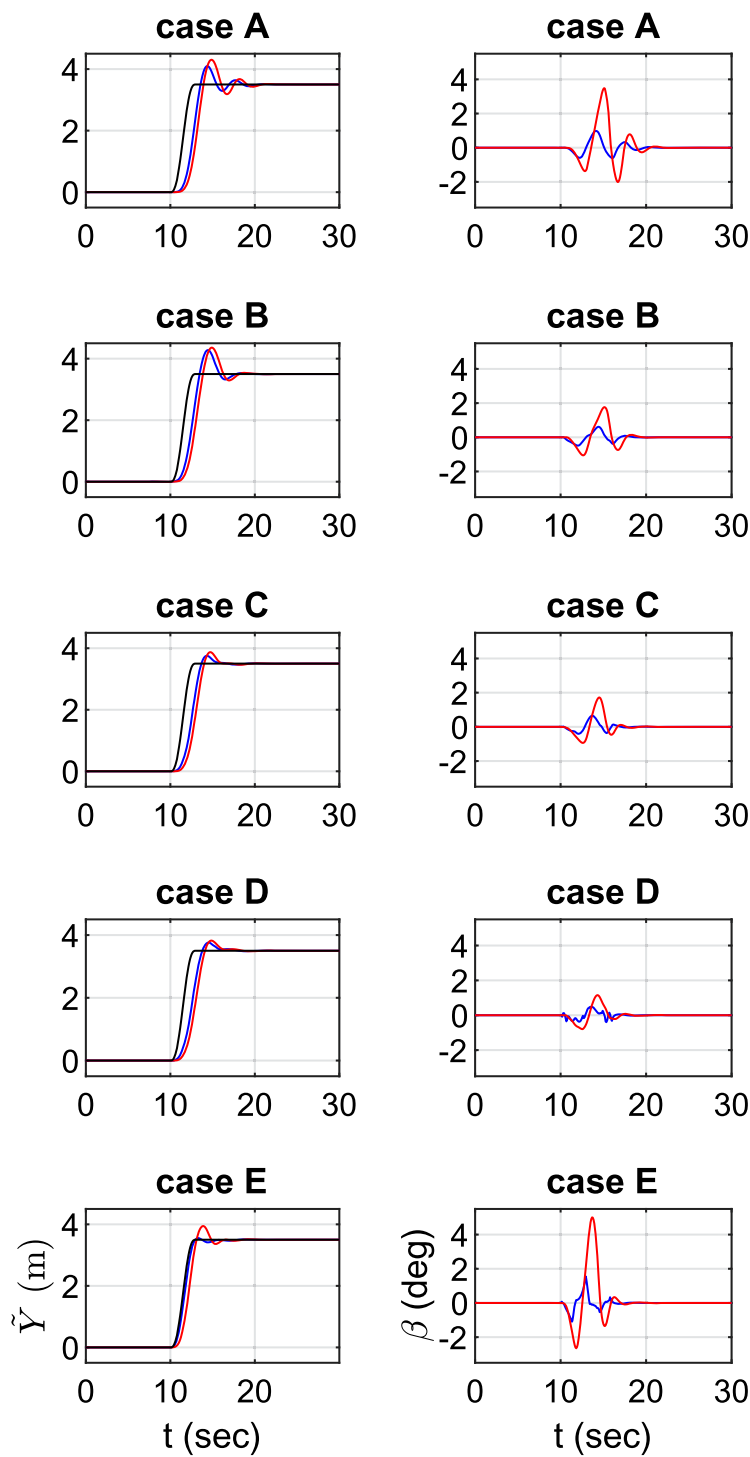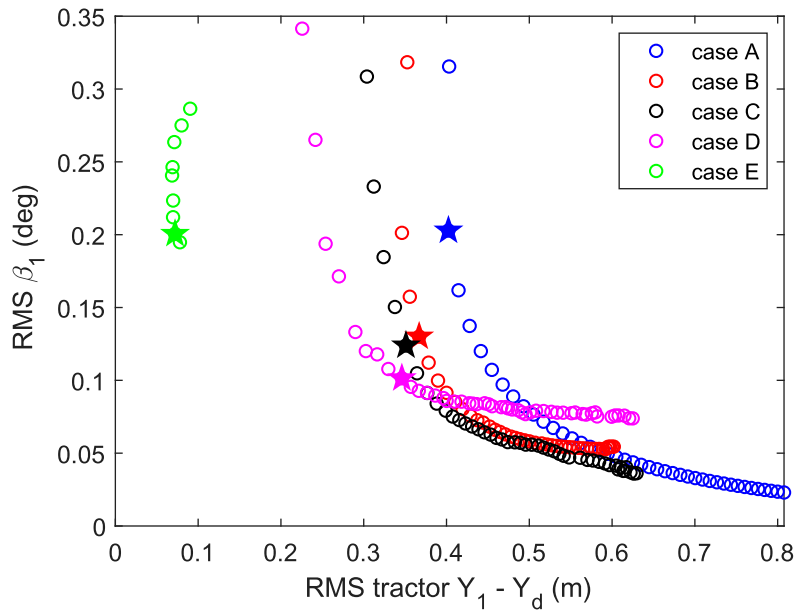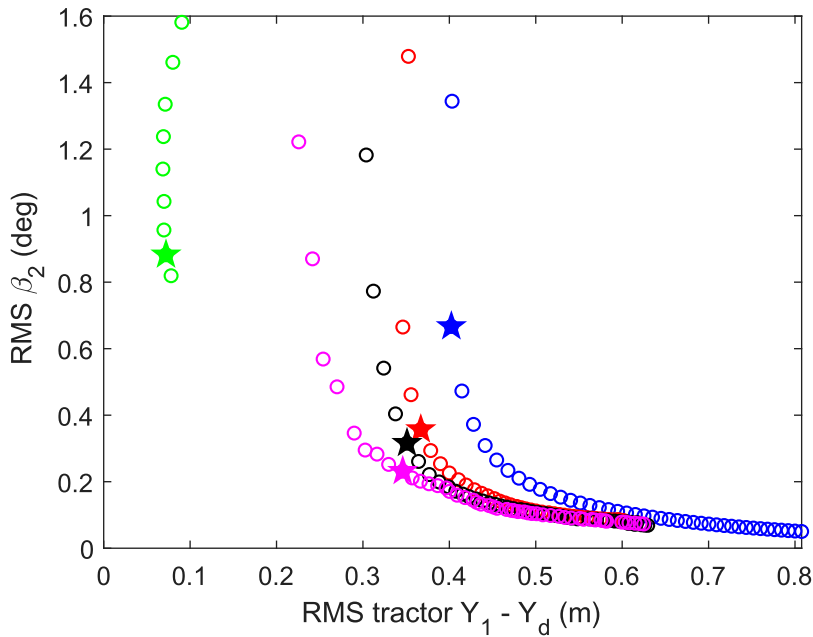
Figure 5. Left column: CG Lateral offset in global coordinates for each case (blue: tractor, red: semitrailer and black: desired). Right column: Sideslip angle for each case (blue: tractor, red: semitrailer)

Figure 6. 2D trade-off plots for evaluating the performance of proposed control systems. (a) tractor CG tracking Root Mean Square (RMS) error versus tractor sideslip angle (b) tractor CG tracking RMS error versus semitrailer sideslip angle. The star in each case corresponds to the time histories shown previously.

It further demonstrates the behaviour of the control system under different parameter settings, specifically τ_p for cases A, B, C, and D and K_{SMC} for Case E. The star symbols are used to indicate the situation in which the time histories are presented in this paper ($\tau_p = 1$ seconds for cases A-D and $K_{SMC} = 0.2$ for case E). There is seen to be a systematic trend toward improvement as control authority is increased. The only exception is in Case D for tractor sideslip, where for longer preview times MHA continues to make use of increased slip angles. However, the overall trend is clear.

In case E, it is seen that we improve the RMS of tracking error as a tracking performance metric while maintaining the RMS values for both tractor and semitrailer sideslip angles consistent with the other cases. When comparing these five cases, it becomes evident that when we give more authority to MHA, manoeuvres with a shorter preview time are possible. It is also clear that MHA has a noticeable benefit even with large preview times. Case E is seen as an outlier because it is most strongly focussed on the path following, and the SMC reference is relatively aggressive. However, it shows that path following is significantly improved, which would likely be the priority in case of a safety-critical lane change.

The yaw rates as well as the front-axle steering angle for each unit are also shown in Figure 7. It is seen that MHA applies higher bandwidth steering signals, and these carry through the yaw rate plots.

Table 2 further reveals that using combined steering and braking in case E results in a significant reduction in tracking error when compared to the other cases. It is likely to be critical to achieve a minimum tracking error in order to successfully execute the obstacle avoidance manoeuvre. The pattern of speed reduction remains consistent in MHA cases. When the peak yaw rates of the tractor and semitrailer are compared, case D performs best. However, as previously stated, the increase in these values for case E is justified because MHA is attempting a drastic lane change within a predetermined time frame. A similar pattern can be seen for the tractor and semitrailer's peak sideslip angles. Also, in case D, the peak articulation angle is smaller than in the other cases.

5. Conclusions and further discussion

This paper is centred around the extension of the Modified Hamiltonian Algorithm (MHA) for a tractor-semitrailer combination. MHA has previously been proposed as a motion control strategy for light vehicles, particularly capable of operating up to the limits of friction.

Controlling the motion of articulated heavy goods vehicles in the nonlinear regions of the tyres is a more challenging task compared to single-unit vehicles. This is because articulated vehicles tend to exhibit unfavourable behaviours when driven near the handling limits. Hence, sophisticated algorithms are required to address these issues. The design of MHA is intended to avoid this problem, with computational load only increasing in a linear way. Using a simple algorithm to estimate the co-states, MHA provides an efficient method of coordinated motion control, whereby each wheel actuator independently minimises its local Hamiltonian function subject to constraints on tyre forces imposed at the wheel level using a nonlinear combined-slip tyre model.

MHA inherently respects control limits by reference to the nonlinear tyre model and the friction ellipse at each wheel. For instance, if the high-level control demands acceleration beyond adhesion limits, the local Hamiltonian minimisation will consistently adhere to
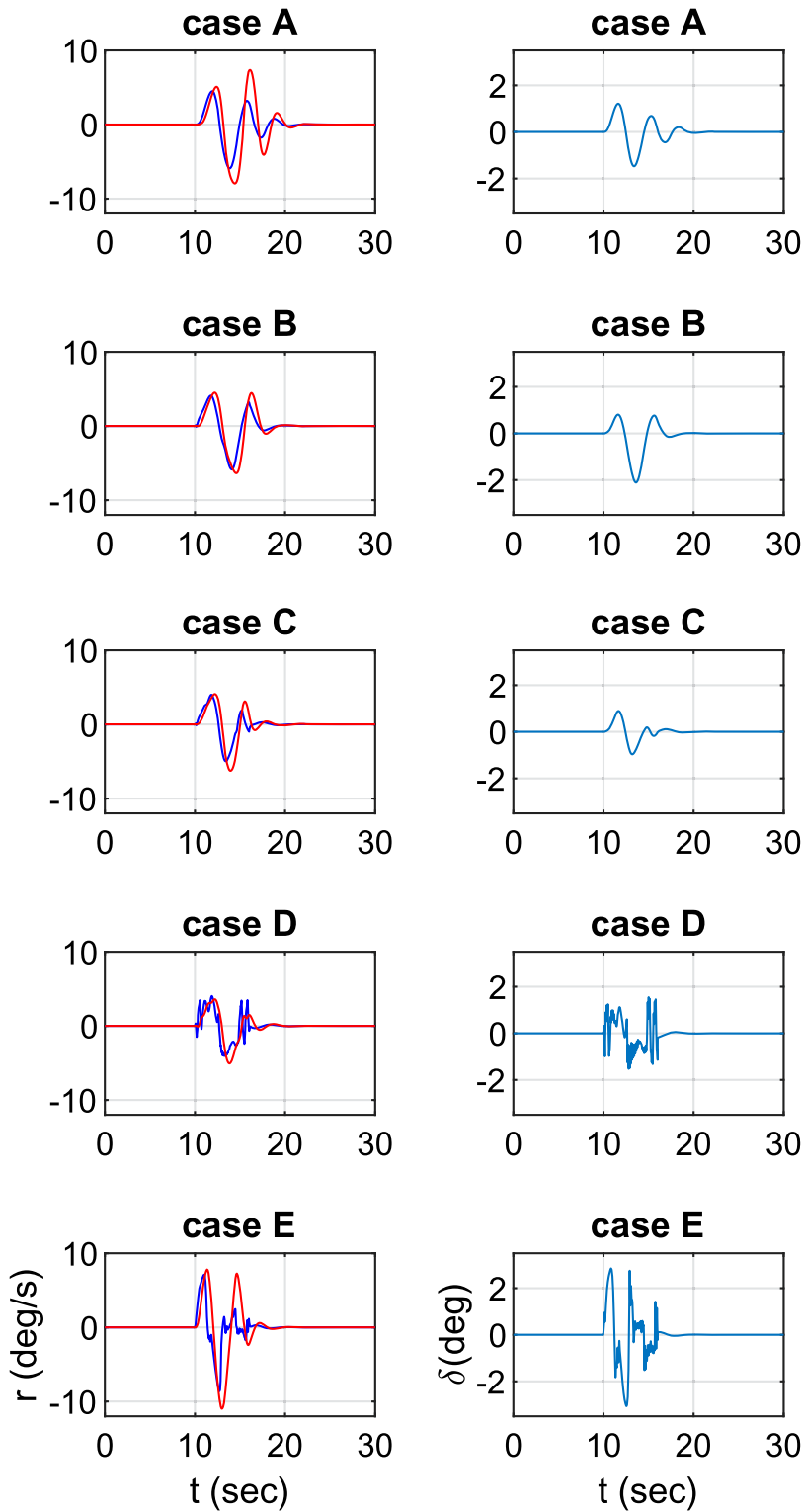
Figure 7. Left column: yaw rates for each case (blue: tractor, red: semitrailer). Right column: front-axle steer angle of the tractor for each case.

Table 2. Motion variables information as well as the speed after the lane change for selected (starred) cases.

Cases	V_2 (km/h)	$\tilde{Y}_1$ (m)	$|r_1|_{max}$ (deg/sec)	$|r_2|_{max}$ (deg/sec)	$|\beta_1|_{max}$ (deg)	$|\beta_2|_{max}$ (deg)	$|\theta|_{max}$ (deg)
A	71.49	0.4	5.9	7.95	0.98	3.48	3.7
B	63.59	0.37	5.86	6.37	0.6	1.76	1.95
C	66.43	0.35	4.96	6.26	0.65	1.7	2.2
D	66.93	0.34	4	5.1	0.48	1.15	1.8
E	65.29	0.07	8.6	10.96	1.55	5	4.65

Note: V_2: speed after lane change $\tilde{Y}_1$: RMS tracking error $(Y_1 - Y_d)$ θ: articulation angle.

the available surface friction limit (μ) where we assume μ is known. In case yaw moment control is prioritised, the emphasis on yaw stability becomes greater, as implemented in the P_Z adaptation rule. To the extent that MHA faithfully approximates the nonlinear optimal controller (via Pontryagin) then stable performance is guaranteed. In simulation (and in practice) MHA is generally found to generate stable dynamics provided μ is not over-estimated, and in case of excessively low surface friction, path following may well be compromised due to the priority control of yaw-sideslip dynamics.

This study has shown that MHA deals consistently with different levels of control authority in the chassis system. It is also worth noting that no parameter tuning was performed in MHA between the different cases.

The PP algorithm is shown to be insufficient to handle a sudden lane change, in contrast to the MHA, which fully comprehends vehicle dynamics and uses integrated steering and braking control to handle the request for a sudden lane change while maintaining the stability of the vehicle combination. The method is shown to work well for an articulated vehicle, a tractor-semitrailer combination, thus improving the vehicle stability and manoeuvrability near the friction limit. While PP may not possess the skill of a human driver, it is expected that the trends likely to be applicable to manually steered evasive manoeuvres.

The research presented in this paper makes a number of original contributions:(i) offering a novel analysis of the trade-off between path following and lateral stability, without being linked to any particular control technique, (ii) demonstrating how increasing the number of available actuators impacts performance within the framework of a particular control method, namely MHA, (iii) presenting the first ever formulation of MHA for articulated vehicles, demonstrating consistency across different levels of actuator authority and benefiting from using a small number of tuning parameters, and (iv) introducing a control design approach that seamlessly transitions between various modes, such as assisting a driver with steering control or operating fully autonomously.

MHA has been applied as an independent motion control algorithm in this paper. In the future it might also serve as a control supervisor for a vehicle's existing motion control algorithm, activating when necessary to achieve defined safety thresholds.

While energy optimisation is not currently included in MHA's distributed optimisation method, this might also be included in the future. The algorithm is seen to excel at operating effectively in safety-critical scenarios where the limits of tyre adhesion may be reached, and in such cases, energy efficiency may not be regarded as significant.

In this study, we have assumed that the controller has prior knowledge of the surface friction coefficient. Consequently, future research should consider the inclusion of friction estimation methods.

Disclosure statement

No potential conflict of interest was reported by the author(s).

References

[1] Kang X, Deng W. Vehicle-trailer handling dynamics and stability control–an engineering review. 2007.
[2] Woodrooffe J, Blower DF, Gordon T, et al. Safety benefits of stability control systems for tractor-semitrailers. Technical report, National Highway Traffic Safety Administration, Washington DC, 2009.
[3] Mobini F, Ghaffari A, Alirezaei M. Non-linear optimal control of articulated-vehicle planar motion based on braking utilizing the state-dependent riccati equation method. Proc Inst Mech Eng, Part D: Journal of Automobile Engineering. 2015;229(13):1774–1787. doi: 10.1177/0954407015571156
[4] Cheng C, Roebuck R, Odhams A, et al. High-speed optimal steering of a tractor–semitrailer. Vehicle Syst Dyn. 2011;49(4):561–593. doi: 10.1080/00423111003615212
[5] Hynén Ulfsjöö C, Westny T. Modeling and lateral control of tractor-trailer vehicles during aggresive maneuvers, 2020.
[6] Jindra F. Handling characteristics of tractor-trailer combinations. SAE Trans. 1966;74:378–394.
[7] Miege AJP, Cebon D. Optimal roll control of an articulated vehicle: theory and model validation. Vehicle Syst Dyn. 2005;43(12):867–884. doi: 10.1080/00423110500217167
[8] Morrison G, Cebon D. Combined emergency braking and turning of articulated heavy vehicles. Vehicle Syst Dyn. 2017;55(5):725–749. doi: 10.1080/00423114.2016.1278077
[9] Ni Z, He Y. Design and validation of a robust active trailer steering system for multi-trailer articulated heavy vehicles. Vehicle Syst Dyn. 2018;57:1545–1571. doi: 10.1080/00423114.2018.1529322
[10] Tian J, Zeng Q, Wang P, et al. Active steering control based on preview theory for articulated heavy vehicles. PLoS ONE. 2021;16(5):e0252098. doi: 10.1371/journal.pone.0252098
[11] Cai H, Xu X. Lateral stability control of a tractor-semitrailer at high speed. Machines. 2022;10(8):716. doi: 10.3390/machines10080716
[12] Marumo Y, Yokota T, Aoki A. Improving stability and lane-keeping performance for multi-articulated vehicles using vector follower control. Vehicle Syst Dyn. 2020;58(12):1859–1872. doi: 10.1080/00423114.2019.1651877
[13] Hou Y, Xu X. High-speed lateral stability and trajectory tracking performance for a tractor-semitrailer with active trailer steering. PLoS ONE. 2022;17(11):e0277358. doi: 10.1371/journal.pone.0277358
[14] Wu D-H, Lin Y-H. Directional response analysis of tractor-trailer with multi-axle-steering carrying liquid load. Technical report, SAE Technical Paper, 2005.
[15] Zong C, Zhu T, Wang C, et al. Multi-objective stability control algorithm of heavy tractor semi-trailer based on differential braking. Chinese J Mech Eng. 2012;25(1):88–97. doi: 10.3901/CJME.2012.01.088
[16] Latif A, Chalhoub N, Pilipchuk V. Control of the nonlinear dynamics of a truck and trailer combination. Nonlinear Dyn. 2020;99(4):2505–2526. doi: 10.1007/s11071-019-05452-1
[17] Oreh SHT, Kazemi R, Azadi S. A sliding-mode controller for directional control of articulated heavy vehicles. Proc Inst Mech Eng, Part D: Journal of Automobile Engineering. 2014;228(3):245–262. doi: 10.1177/0954407013503628
[18] Oreh SHT, Kazemi R, Azadi S. A new desired articulation angle for directional control of articulated vehicles. Proc Inst Mech Eng, Part K: Journal of Multi-Body Dynamics. 2012;226(4):298–314.
[19] Sharifzadeh M, Farnam A, Senatore A, et al. Delay-dependent criteria for robust dynamic stability control of articulated vehicles. In: Advances in Service and Industrial Robotics: Proceedings of the 26th International Conference on Robotics in Alpe-Adria-Danube Region, RAAD 2017. Springer; 2018. p. 424–432. Polytechnic University of Turin, Italy.

[20] Yang X, Song J, Gao J. Fuzzy logic based control of the lateral stability of tractor semitrailer vehicle. Math Problems Eng. 2015;2015:1–16.

[21] Yang X, Xiong J. Nonlinear yaw dynamics analysis and control for the tractor-semitrailer vehicle. Int J Heavy Veh Syst. 2013;20(3):253–288. doi: 10.1504/IJHVS.2013.054787

[22] Zanchetta M, Tavernini D, Sorniotti A, et al. Trailer control through vehicle yaw moment control: theoretical analysis and experimental assessment. Mechatronics. 2019;64:102282. doi: 10.1016/j.mechatronics.2019.102282

[23] Elhemly MAE, Fayed MAE, Elmaihy AAE. Tractor–semitrailer jackknifing elimination using semitrailer differential braking technique. Int J Heavy Veh Syst. 2013;20(1):19–34. doi: 10.1504/IJHVS.2013.051100

[24] Yang X. Optimal reconfiguration control of the yaw stability of the tractor-semitrailer vehicle. Math Probl Eng. 2012;2012:602502. doi: 10.1155/mpe.v2012.1

[25] Bai Z, Lu Y, Li Y. Method of improving lateral stability by using additional yaw moment of semi-trailer. Energies. 2020;13(23):6317. doi: 10.3390/en13236317

[26] Abroshan M, Hajiloo R, Hashemi E, et al. Model predictive-based tractor-trailer stabilisation using differential braking with experimental verification. Vehicle Syst Dyn. 2021;59(8):1190–1213. doi: 10.1080/00423114.2020.1744024

[27] Barbosa FM, Marcos LB, da Silva MM, et al. Robust path-following control for articulated heavy-duty vehicles. Control Eng Practice. 2019;85:246–256. doi: 10.1016/j.conengprac.2019.01.017

[28] Zhang Y, Khajepour A, Ataei M. A universal and reconfigurable stability control methodology for articulated vehicles with any configurations. IEEE Trans Vehicular Technol. 2020;69(4):3748–3759. doi: 10.1109/TVT.25

[29] Liu L, Wang B, He Y. Research on path-tracking control of articulated vehicle with a trailer based on advanced model prediction control strategy. lateral. 2021;20:1.

[30] Sharma T, He Y. Design of a tracking controller for autonomous articulated heavy vehicles using a nonlinear model predictive control technique. Proceedings of the Institution of Mechanical Engineers, Part K: Journal of Multi-body Dynamics. 2024: doi:10.1177/14644193241232353

[31] Uhlén K, Nyman P, Eklöv J, et al. Coordination of actuators for an a-double heavy vehicle combination using control allocation. In: 17th International IEEE Conference on Intelligent Transportation Systems (ITSC). IEEE; 2014. p. 641–648. Qingdao, China.

[32] Sinigaglia A, Tagesson K, Falcone P, et al. Coordination of motion actuators in heavy vehicles using model predictive control allocation. In: 2016 IEEE Intelligent Vehicles Symposium (IV). IEEE; 2016. p. 590–596. Gothenburg, Sweden.

[33] Arikere A, Yang D, Klomp M. Optimal motion control for collision avoidance at left turn across path/opposite direction intersection scenarios using electric propulsion. Vehicle Syst Dyn. 2019;57(5):637–664. doi: 10.1080/00423114.2018.1478107

[34] Gao Y, Gordon T, Lidberg M. Optimal control of brakes and steering for autonomous collision avoidance using modified hamiltonian algorithm. Vehicle Syst Dyn. 2019;57(8):1224–1240.

[35] Asiabar AN, Gordon T, Gao Y, et al. Integrated motion control for heavy goods vehicles using multiple actuators. In: The IAVSD International Symposium on Dynamics of Vehicles on Roads and Tracks. Springer; 2023. Ottawa, Canada.

[36] Gordon T, Gao Y. A flexible hierarchical control method for optimal collision avoidance. In: Proceedings of the 16th International Conference on Mechatronics-Mechatronika 2014. IEEE; 2014. p. 318–324. Brno, Czech Republic.

[37] Gao Y, Lidberg M, Gordon T. Modified hamiltonian algorithm for optimal lane change with application to collision avoidance. MM Sci J. 2015;2015:576–584. doi: 10.17973/MMSJ

[38] Gao Y. Vehicle motion and stability control at the limits of handling via the modified Hamiltonian algorithim: methodology and applications [dissertation], University of Lincoln, 2018.

[39] Hellstrom T, Ringdahl O. Follow the past: a path-tracking algorithm for autonomous vehicles. Int J Vehicle Auton Syst. 2006;4(2-4):216–224. doi: 10.1504/IJVAS.2006.012208

[40] Elbanhawi M, Simic M, Jazar R. Receding horizon lateral vehicle control for pure pursuit path tracking. J Vibration Control. 2018;24(3):619–642. doi: 10.1177/1077546316646906

[41] Gudetti J, Panchal T, Bastiaan J. An analysis of the vehicle dynamics behind pure pursuit and stanley controllers. Technical report, SAE Technical Paper, 2023.
[42] Kim S, Lee J, Han K, et al. Vehicle path tracking control using pure pursuit with mpc-based look-ahead distance optimization. IEEE Trans Vehicular Technol. 2023;73(1):53–66. doi: 10.1109/TVT.2023.3304427
[43] Ohta H, Akai N, Takeuchi E, et al. Pure pursuit revisited: field testing of autonomous vehicles in urban areas. In: 2016 IEEE 4th International Conference on Cyber-Physical Systems, Networks, and Applications (CPSNA). IEEE; 2016. p. 7–12. Nagoya, Japan.
[44] Rajamani R. Vehicle dynamics and control. New York: Springer Science & Business Media; 2011.
[45] Norouzi A, Kazemi R, Azadi S. Vehicle lateral control in the presence of uncertainty for lane change maneuver using adaptive sliding mode control with fuzzy boundary layer. Proc Inst Mech Eng, Part I: Journal of Systems and Control Engineering. 2018;232(1): 12–28.
[46] Kirk DE. Optimal control theory: an introduction. Englewood Cliffs, New Jersey: Courier Corporation; 2004.
[47] Yang D, Gordon TJ, Jacobson B, et al. Quasi-linear optimal path controller applied to post impact vehicle dynamics. IEEE Trans Intell Transp Syst. 2012;13(4):1586–1598. doi: 10.1109/TITS.2012.2204875
[48] Slotine JE, Li W. Applied nonlinear control. Vol. 199. Prentice Hall Englewood Cliffs, New Jersey; 1991.
[49] Meirovitch L. Methods of analytical dynamics. New York: Courier Corporation; 2010.
[50] Fors V. Autonomous vehicle maneuvering at the limit of friction [dissertation]. 2020.

Appendices

Appendix 1 Vehicle specification

The schematic of the tractor-semitrailer combination is shown in Figure A1. The list of parameters used in this paper is also listed in Table A1 as:
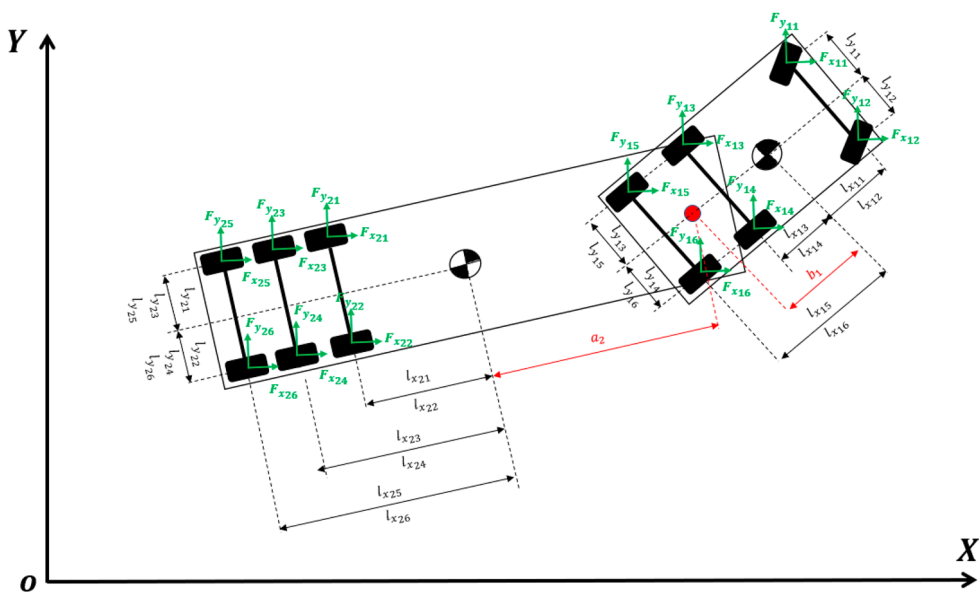

Figure A1. Schematic of the tractor-semitrailer combination.

Table A1. Parameters for Tractor-semitrailer combination.

Vehicle parameters	Symbol	Value	Unit
Mass (tractor)	m_1	8808	kg
Mass (semitrailer)	m_2	39000	kg
Yaw moment of inertia (tractor)	I_{zz_1}	41389	kgm^2
Yaw moment of inertia (semitrailer)	I_{zz_2}	606165	kgm^2
Longitudinal distance from tractor CG to articulation joint	b_1	1.64	m
Longitudinal distance from semitrailer CG to articulation joint	a_2	5.5	m
Longitudinal distance from tractor CG to the 1st axle	$l_{x_{11,12}}$	2.75	m
Longitudinal distance from tractor CG to the 2nd axle	$l_{x_{13,14}}$	0.95	m
Longitudinal distance from tractor CG to the 3rd axle	$l_{x_{15,16}}$	2.32	m
Longitudinal distance from semitrailer CG to the 1st axle	$l_{x_{21,22}}$	0.89	m
Longitudinal distance from semitrailer CG to the 2nd axle	$l_{x_{23,24}}$	2.2	m
Longitudinal distance from semitrailer CG to the 3rd axle	$l_{x_{25,26}}$	3.5	m
Half of the track width (tractor)	$l_{y_{11,13,15}}$	1.09	m
Half of the track width (semitrailer)	$l_{y_{21,23,25}}$	1.02	m
Wheel radius	R_w	0.49	m
Steering actuator time constant	τ_s	0.02	sec
Braking actuator time constant	τ_b	0.1	sec

Appendix 2 Full EOM

The generalised forces Q_{q_k}, can be written in terms of tyre forces via:

$$\vec{Q} = \sum_{i=1}^{2} \sum_{j=1}^{6} [B]_{ij} \vec{F}_{ij} \tag{A1}$$

Therefore the EOM in terms of tyre forces as inputs to the system are as follows:

$$
\begin{bmatrix}
m_1 + m_2 & 0 & m_2 b_1 \sin\psi_1 & m_2 a_2 \sin\psi_2 \\
0 & m_1 + m_2 & -m_2 b_1 \cos\psi_1 & -m_2 a_2 \cos\psi_2 \\
m_2 b_1 \sin\psi_1 & -m_2 b_1 \cos\psi_1 & I_{zz_1} + m_2 b_1^2 & b_1 m_2 a_2 \cos(\psi_1 - \psi_2) \\
m_2 a_2 \sin\psi_2 & -m_2 a_2 \cos\psi_2 & b_1 m_2 a_2 \cos(\psi_1 - \psi_2) & I_{zz_2} + m_2 a_2^2
\end{bmatrix}
\begin{bmatrix}
\ddot{X}_1 \\
\ddot{Y}_1 \\
\ddot{\psi}_1 \\
\ddot{\psi}_2 \\
\ddot{\psi}_3
\end{bmatrix}
$$

$$
+ \begin{bmatrix}
b_1 m_2 \cos\psi_1 \dot{\psi}_1^2 + a_2 m_2 \cos\psi_2 \dot{\psi}_2^2 \\
b_1 m_2 \sin\psi_1 \dot{\psi}_1^2 + a_2 m_2 \sin\psi_2 \dot{\psi}_2^2 \\
a_2 b_1 m_2 \sin(\psi_1 - \psi_2) \dot{\psi}_2^2 \\
-a_2 b_1 m_2 \sin(\psi_1 - \psi_2) \dot{\psi}_1^2
\end{bmatrix}
= \begin{bmatrix}
\vec{b}_{11} & \vec{0}_{1 \times 12} \\
\vec{0}_{1 \times 12} & \vec{b}_{22} \\
\vec{b}_{31} & \vec{b}_{32} \\
\vec{b}_{41} & \vec{b}_{42}
\end{bmatrix}
\begin{bmatrix}
\vec{F}_x \\
\vec{F}_y
\end{bmatrix}
$$

where

$$\vec{b}_{11} = \vec{b}_{22} = \begin{bmatrix} 1 & 1 & 1 & 1 & 1 & 1 & 1 & 1 & 1 & 1 & 1 & 1 \end{bmatrix}_{1 \times 12}$$

$$\vec{b}_{31} = \left[\left\{ -\vec{L}_{x_1} \sin\psi_1 - \vec{L}_{y_1} \cos\psi_1 \right\}_{1 \times 6} \quad \left\{ b_1 \sin\psi_1 \right\}_{1 \times 6} \right]_{1 \times 12}$$

$$\vec{b}_{32} = \left[\left\{ \vec{L}_{x_1} \cos\psi_1 - \vec{L}_{y_1} \sin\psi_1 \right\}_{1 \times 6} \quad \left\{ -b_1 \cos\psi_1 \right\}_{1 \times 6} \right]_{1 \times 12}$$

$$\vec{b}_{41} = \left[\vec{0}_{1\times 6} \quad \left\{ \{a_2 - \vec{L}_{x_2}\} \sin \psi_2 - \vec{L}_{y_2} \cos \psi_2 \right\}_{1\times 6} \right]_{1\times 12}$$

$$\vec{b}_{42} = \left[\vec{0}_{1\times 6} \quad \left\{ \{-a_2 + \vec{L}_{x_2}\} \cos \psi_2 - \vec{L}_{y_2} \sin \psi_2 \right\}_{1\times 6} \right]_{1\times 12}$$

$$\vec{F}_x = \begin{bmatrix} F_{x_{11}} & F_{x_{12}} & F_{x_{13}} & F_{x_{14}} & F_{x_{15}} & F_{x_{16}} & F_{x_{21}} & F_{x_{22}} & F_{x_{23}} & F_{x_{24}} & F_{x_{25}} & F_{x_{26}} \end{bmatrix}^T$$

$$\vec{F}_y = \begin{bmatrix} F_{y_{11}} & F_{y_{12}} & F_{y_{13}} & F_{y_{14}} & F_{y_{15}} & F_{y_{16}} & F_{y_{21}} & F_{y_{22}} & F_{y_{23}} & F_{y_{24}} & F_{y_{25}} & F_{y_{26}} \end{bmatrix}^T$$

Appendix 3 Calculation of the desired yaw rate and the desired sideslip angle rate [37,50]

In MHA algorithm, the desired yaw rate $\dot{\psi}^d$ is determined online based on anticipated path curvature and desired body sideslip $\dot{\beta}^d$ within the algorithm. Comparing this to the actual yaw rate, a corresponding desired yaw moment is found, and trade-off parameters P_Z are adjusted to guide the actual yaw motion towards the reference as:

$$\dot{\psi}_i^d = \dot{\phi}_i^d + \dot{\beta}_i^d \tag{A2}$$

where $\dot{\beta}_i^d$ is obtained using Hamiltonian minimisation and $\dot{\phi}_i$ is related to the path curvature calculated based on desired acceleration in path coordinates as:

$$\dot{\phi}_i^d = \frac{-a_{X_d} \sin \phi_i + a_{Y_d} \cos \phi_i}{\sqrt{v_x^2 + v_y^2}} \tag{A3}$$

where $\phi_i = \psi_i - \beta_i$ is the path angle related to each unit and $\dot{\phi}_i^d$ is the desired path angle change found from desired acceleration vector. Regarding the semitrailer, $\dot{\phi}_2^d$ is assumed to be zero because the semitrailer's primary goal is to follow the tractor's motion rather than to follow a reference. As a result, only the stabilisation term is considered when calculating the desired yaw rate for the semitrailer. Comparing the desired yaw rate calculated from Equation (A2) to the actual yaw rate, a corresponding desired yaw moment is found:

$$\tau \frac{d\dot{\psi}_i}{dt} = \dot{\psi}_i^d - \dot{\psi}_i \tag{A4}$$

$$M_{z\,i}^d = \frac{I_{zz_i}}{\tau_i} \left(\dot{\psi}_i^d - \dot{\psi}_i \right) \tag{A5}$$

where τ is a time constant and I_{zz_i} is the yaw moment of inertia of each unit.

The vehicle sideslip angle should also be modified to improve the slip angles for rear tyres as there is no steering on the semitrailer and the rear wheels of the tractor. Therefore, in a similar way to finding the desired steering angle we have,

$$H_\beta = \sum_{i=1}^{2} \sum_{j=1}^{6} \frac{\partial H_{ij}}{\partial \beta_i} = \sum_{i=1}^{2} \sum_{j=1}^{6} \frac{\partial H_{ij}}{\partial \alpha_{ij}} \cdot \frac{\partial \alpha_{ij}}{\partial \beta_i} \approx \sum_{i=1}^{2} \sum_{j=1}^{6} \frac{\partial H_{ij}}{\partial \alpha_{ij}} \tag{A6}$$

The desired side slip angle rate can be expressed as:

$$\dot{\beta}^d = \begin{cases} K_{\beta_1} \text{sign}(\beta) & |\beta| > \beta_2 \\ 0 & |\beta| > \beta_1 \cap \beta H_\beta < 0 \\ -K_{\beta_2} \tanh(K_{\beta_2} H_\beta) & \text{otherwise} \end{cases} \tag{A7}$$

where β_1 and β_2 are lower and upper thresholds for sideslip angle. The computed target sideslip angle rate is used to determine the desired yaw rate in (A2).